Dynamic motion and freezing of polaronic local structures in a colossal-magnetoresistive perovskite manganite $La_{0.7}Ca_{0.3}MnO_3$ detected with radioactive nuclei

W. Sato,[1,2] S. Komatsuda,[3] H. Shimizu,[2] R. Moriichi,[2] S. Abe,[1,2] S. Watanabe,[2] S. Komatsu,[2] T. Terai,[4] S. Kawata,[5] and Y. Ohkubo[6]

[1]*Institute of Science and Engineering, Kanazawa University, Kanazawa, Ishikawa 920–1192, Japan*
[2]*Graduate School of Natural Science and Technology, Kanazawa University, Kanazawa, Ishikawa 920–1192, Japan*
[3]*Institute of Human and Social Sciences, Kanazawa University, Kanazawa, Ishikawa 920-1192, Japan*
[4]*Graduate School of Engineering, Osaka University, Suita, Osaka 565–0781, Japan*
[5]*Department of Chemistry, Faculty of Science, Fukuoka University, Fukuoka, Fukuoka 814-0180, Japan*
[6]*Institute for Integrated Radiation and Nuclear Science, Kyoto University, Kumatori, Osaka 590-0494, Japan*

(Received 30 July 2018; revised manuscript received 2 October 2019; published 15 November 2019)

The magnetic hyperfine field and electric field gradients at a radioactive impurity probe of ^{111}Cd($\leftarrow {}^{111m}$Cd) occupying the La/Ca *A* site in a perovskite manganaite $La_{0.7}Ca_{0.3}MnO_3$ ($T_C \sim 250$ K) were measured by means of time-differential perturbed angular correlation (TDPAC) spectroscopy. In the paramagnetic-insulator phase at room temperature, the ^{111}Cd($\leftarrow {}^{111m}$Cd) probes are distributed in two different environments: distorted and less distorted sites; whereas in the ferromagnetic-metal phase below T_C, the oscillatory structure of the distorted component vanishes from the TDPAC function. The vanishing of the oscillation is ascribable to dynamic motion of polarons dragged by conduction electrons induced by the double exchange interaction. In liquid helium, the dynamic motion freezes, leaving averaged local distortion. The dynamic motion and freezing of local structures associated with the colossal-magnetoresistance phase transition to the ferromagnetic phase is discussed on the basis of temperature-dependent electromagnetic fields at the probe nuclei of the *A* site ions.

DOI: 10.1103/PhysRevB.100.184111

I. INTRODUCTION

Doped perovskite manganese oxides ($R_{1-x}A_xMnO_3$, where *R* and *A* stand for rare earth and alkaline earth metal elements, respectively) are one of the most promising materials applicable to future spintronic devices. Since the discovery of the effect of colossal magnetoresistance (CMR) at high temperature [1], much effort has been focused on the understanding of the origin of the phenomenon so as to raise their magnetic property and electric conductivity [2]. The CMR mechanism is basically explained in the framework of the double exchange interaction arising from the e_g electron hopping between heterovalent $Mn^{3+}-Mn^{4+}$ ions [3,4]. In addition, many papers suggest that different phenomena such as charge and orbital ordering should be taken into account for the explanation of the physical properties of manganites. It is also reported that existence of nanoscale inhomogeneous structures strongly affects their magnetic properties [5,6]. For a detailed examination of the magnetotransport phenomenon of manganese oxides, therefore, microscopic information of local sites is essential. In this respect, atomic scale observation of the *A* site is very important because magnetoresistance of $R_{1-x}A_xMnO_3$ is governed largely by doping of *A*-site ions [4,7–9]. Information on an electromagnetic phenomenon occurring at the *A* site around the phase transition temperature is especially important for materials design of functional devices.

From this point of view, we employed time-differential perturbed angular correlation (TDPAC) spectroscopy for the present study. The TDPAC method is a powerful nuclear spectroscopic technique, providing atomic level information on local structures and/or internal fields at the radioactive nuclear probe through hyperfine interactions between the nuclei and the surrounding spins and charge distribution [10,11]. Thus, this spectroscopy fulfills the present requirement for the investigation of a specific local site. Taking this advantage, we measured in our previous work the local electromagnetic field at the *A* site in a perovskite manganite $La_{0.7}Ca_{0.3}MnO_3$ with the ^{140}Ce($\leftarrow {}^{140}$La) probe [12]. In the study, we succeeded in observing a dramatic change in the hyperfine field at the probe nucleus residing in the La/Ca *A* site below $T_C \sim 250$ K, demonstrating that the magnetic transition of Mn at the *B* site largely affects the local field at the *A* site [13].

The next stage of this study is to clarify the structural change at the *A* site in $La_{0.7}Ca_{0.3}MnO_3$ at temperatures above and below T_C. As regards the local electronic structure, the formation of polarons in the vicinity of Mn ions has been discussed in the literature [14,15]. Because they cause distortion of their neighboring structure, their formation and behavior could also be detected via electric quadrupole interaction between the adjacent probe nucleus and the electric field gradient (EFG) produced by the polarons. For clear information on the local structure, in the present work, we adopted the ^{111}Cd($\leftarrow {}^{111m}$Cd) probe because it is nonmagnetic and sensitive to the EFG. From the temperature dependence of the EFG at the ^{111}Cd($\leftarrow {}^{111m}$Cd) probe occupying the La/Ca *A* site, in this paper, we discuss the formation and dynamics of Jahn-Teller (JT) polarons associated with the effect of

 ©2019 American Physical Society

electric conductivity. In addition to the information of the local structure, we also discuss the contrastive marked change in the local field at the ^{140}Ce nucleus observed in our previous work [12].

II. EXPERIMENTS

Powder $La_{0.7}Ca_{0.3}MnO_3$ was synthesized by a conventional solid-state reaction in air [16,17]. The stoichiometric amount of starting powder materials (MnO_2, La_2O_3, and $CaCO_3$) was thoroughly mixed in a mortar. The powder mixture was calcined on a platinum plate at 1273 K for 12 h. After cooling down to room temperature, the sample was again ground to uniformity, and it was pressed into a disk. The disk was then sintered on a platinum plate at 1473 K for 96 h. For the characterization of the synthesized $La_{0.7}Ca_{0.3}MnO_3$, powder x-ray diffraction (XRD) patterns were obtained at different temperatures using Cu-Kα radiation, and magnetization measurements were carried out to investigate bulk magnetic behavior of the sample.

About 3 mg of cadmium oxide (CdO) enriched with ^{110}Cd was irradiated with thermal neutrons in the research reactor of Kyoto University (KUR) with a flux of 5.5×10^{12} cm^{-2} s^{-1} typically for 60 min, and radioactive ^{111m}Cd was generated by the ^{110}Cd$(n, \gamma)^{111m}$Cd reaction. For the introduction of the radioactive nuclear probe into the sample, the neutron-irradiated CdO powder was then added into 250 mg of $La_{0.7}Ca_{0.3}MnO_3$ powder sample synthesized above. After being mixed in a mortar, the mixture was pressed into a disk and sintered in air at 1373 K for 45 min, and TDPAC measurements were performed in the way described below. Through the introduction of the ^{111m}Cd probe, the pristine $La_{0.7}Ca_{0.3}MnO_3$ was inevitably doped with 2 at. % of nonradioactive Cd ions together with the probe; this treatment possibly brings about substantial change in the physical property of the sample. In order to examine the possibility, we synthesized an identical sample of 2 at. % nonradioactive Cd-doped $La_{0.7}Ca_{0.3}MnO_3$ through the same synthetic procedure taken for the introduction of the ^{111m}Cd probe, and the powder XRD pattern, magnetization curves and resistivity curves were obtained for the synthesized sample.

TDPAC measurements were carried out for the sample containing the ^{111}Cd($\leftarrow {}^{111m}$Cd) probe on the 151–245 keV cascade γ rays with the intermediate states of $I = 5/2$ having half-life of 85.0 ns [18]. A simplified decay scheme of the probe is shown in Fig. 1(a). For the γ-ray detection, a conventional four detector system of BaF_2 scintillation detectors was adopted to observe delayed coincidence events of the cascade at π and $\pi/2$ radians. In the present work, we obtained the directional anisotropy of the cascade as a function of the time interval of the γ-ray emissions by the following relation:

$$A_{22}G_{22}(t) = \frac{2[N(\pi, t) - N(\pi/2, t)]}{N(\pi, t) + 2N(\pi/2, t)}, \quad (1)$$

where A_{22} denotes the angular correlation coefficient representing the magnitude of the directional anisotropy of the cascade γ rays, $G_{22}(t)$ is the time-differential perturbation factor as a function of the time interval, t, between the cascade γ-ray emissions, and $N(\theta, t)$ are the number of the delayed coincidence events observed at an angle, θ. Low-temperature TDPAC functions were obtained with the sample sunk in respective cryogenic liquids: dry-ice containing ethanol (201 K), liquid nitrogen (77 K), and liquid helium (4.2 K).

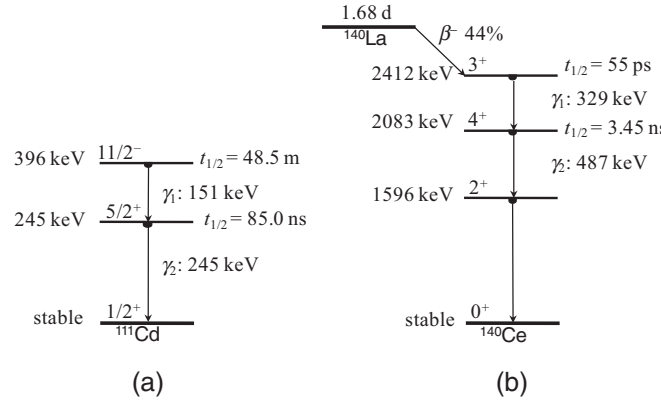

FIG. 1. Simplified decay schemes (a) of the ^{111}Cd($\leftarrow {}^{111m}$Cd) and (b) of the ^{140}Ce($\leftarrow {}^{140}$La) probes. The latter is displayed for reference for the discussion in Sec. III B 2.

III. RESULTS AND DISCUSSION

A. Sample characterization

Structural characterization of the synthesized polycrystalline $La_{0.7}Ca_{0.3}MnO_3$ was carried out by the powder XRD patterns. The room-temperature diffractogram is shown in Fig. 2(a). The diffraction peaks demonstrate that an orthorhombic perovskite structure is formed as expected. Temperature dependence of the angle of a diffraction peak observed at $2\theta \sim 58.55$ degrees shown in Fig. 2(b) evidences the phase transition at 250 K, which demonstrates that the structural change is coupled with the magnetic transition stated just below.

Typical magnetization curves of zero-field-cooled (ZFC) and field-cooled (FC) runs for the sample are shown in Fig. 3. The abrupt change in the magnetization curve at around 250 K indicates the paramagnetic-ferromagnetic phase transition. These structural and magnetic characterizations corroborate the successful synthesis of $La_{0.7}Ca_{0.3}MnO_3$ reported in the literature [17].

The powder XRD pattern, magnetization curves and resistivity curves for the 2 at. % nonradioactive Cd-doped $La_{0.7}Ca_{0.3}MnO_3$ are shown in Fig. 4. Any secondary phase was detected in the XRD pattern shown in Fig. 4(a), suggesting that Cd ions were successfully introduced in the matrix as solid solute. The temperature dependence of the M/H curves in Fig. 4(b) shows a similar trend to that of the pristine $La_{0.7}Ca_{0.3}MnO_3$ shown in Fig. 3, suggesting that paramagnetic-ferromagnetic phase transition takes place at T_C. The slight shift of T_C is ascribable to the effect of the Cd doping. As for the resistivity shown in Fig. 4(c), we can see a typical temperature variation expected for the CMR effect at around T_C. The shoulder-like undulation at around 260 K may

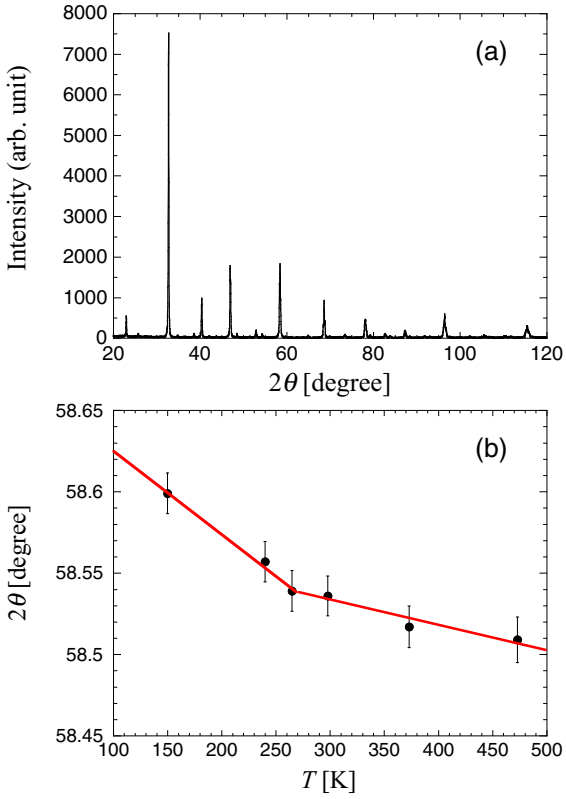

FIG. 2. (a) Powder x-ray diffraction pattern of $La_{0.7}Ca_{0.3}MnO_3$ at room temperature, and (b) temperature dependence of the diffraction angle for the peak at $2\theta \sim 58.55$ degrees. The solid line is a guide to the eye.

also be attributed to the effect of the Cd doping. Although slight changes can be pointed out for both measurements, it was found that Cd-doping does not substantially disturb the original property of $La_{0.7}Ca_{0.3}MnO_3$. The results of the TDPAC measurements are discussed based on these observations.

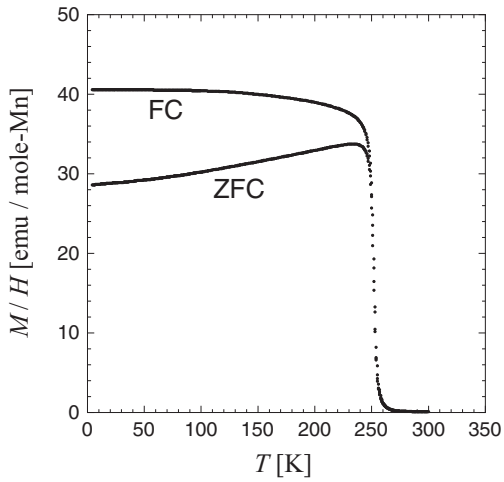

FIG. 3. Magnetization curves for $La_{0.7}Ca_{0.3}MnO_3$ taken zero field cooled (ZFC) and field cooled (FC) at 100 Oe.

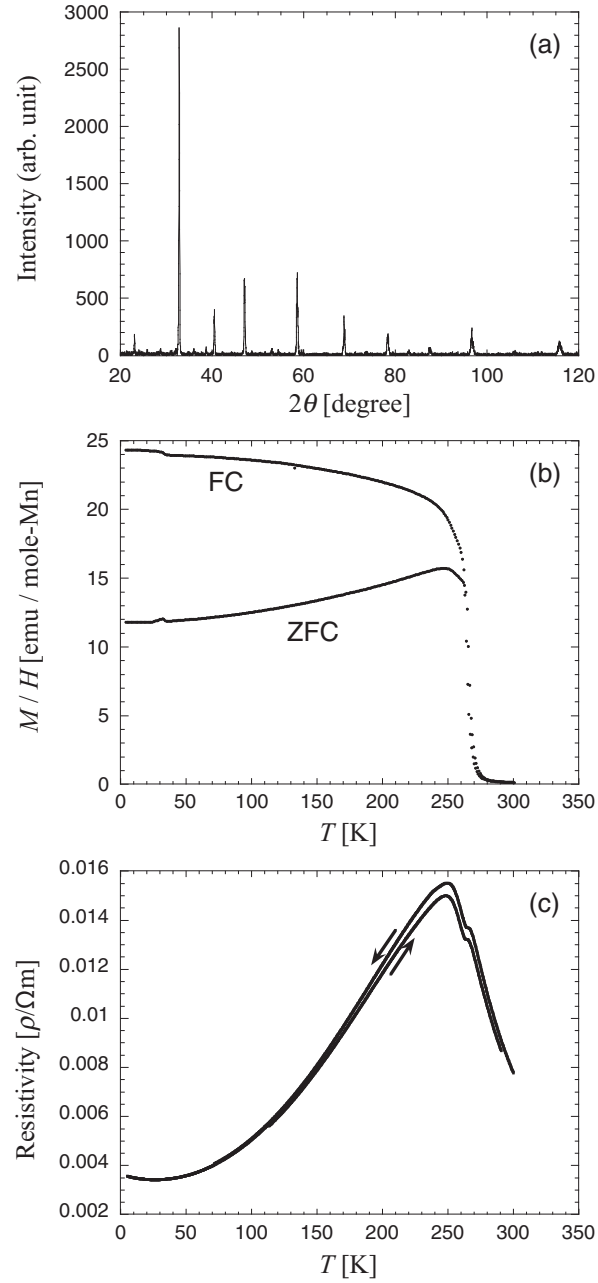

FIG. 4. (a) Powder XRD pattern, (b) magnetization curves taken zero field cooled (ZFC) and field cooled (FC) at 100 Oe and (c) resistivity curves observed for 2 at. % Cd-doped $La_{0.7}Ca_{0.3}MnO_3$.

B. Electromagnetic fields at the *A* site

1. Temperature-dependent local structures at the ^{111}Cd($\leftarrow$ ^{111m}Cd) probe sites

Figure 5 shows the TDPAC functions of the ^{111}Cd($\leftarrow$ ^{111m}Cd) probe in $La_{0.7}Ca_{0.3}MnO_3$ measured at different temperatures. As is obvious from Fig. 4(b), the sample is in the paramagnetic state at room temperature. The room-temperature function in Fig. 5(a) was therefore fitted with the following perturbation factor $G_{22}(t)$ assuming only electric quadrupole interaction between the probe nucleus on the intermediate state of the cascade ($I = 5/2$) and the extranuclear charge distribution due to the paramagnetic nature of the

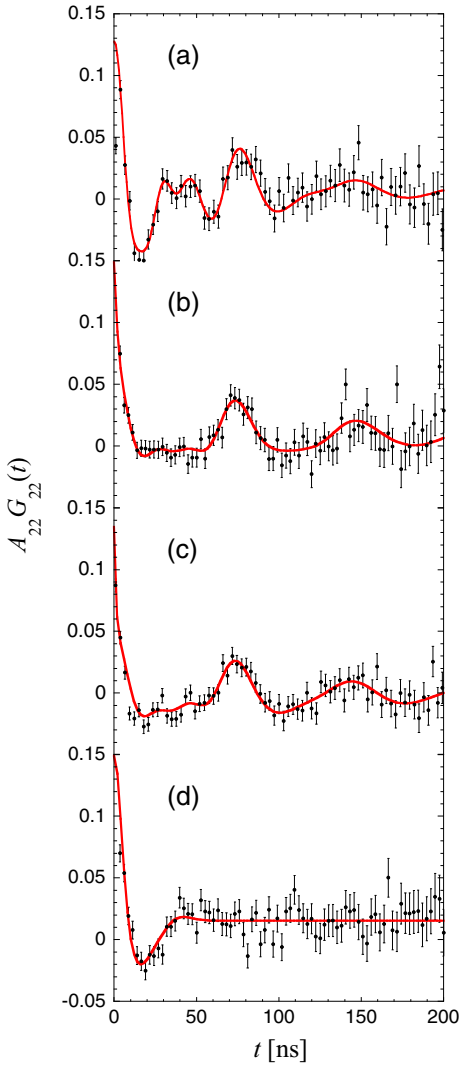

FIG. 5. TDPAC functions of ^{111}Cd($\leftarrow {}^{111m}$Cd) in polycrystalline $La_{0.7}Ca_{0.3}MnO_3$ measured (a) at room temperature, (b) at 201 K, (c) at 77 K, and (d) at 4.2 K.

sample:

$$G_{22}(t) = \sigma_{2,0} + \sum_{n=1}^{3} \sigma_{2,n} \cos(\omega_n t). \tag{2}$$

In Eq. (2), the amplitudes $\sigma_{2,n}$ are functions only of the asymmetry parameter $\eta = (V_{xx} - V_{yy})/V_{zz} (0 \leqslant \eta \leqslant 1)$ for the principal axes of the EFG chosen as $|V_{xx}| \leqslant |V_{yy}| \leqslant |V_{zz}|$. An EFG can be described by using the two tensor parameters V_{zz} and η for the diagonalized symmetric EFG tensor. The frequencies ω_n are related to the electric quadrupole frequency,

$$\omega_Q = -\frac{eQV_{zz}}{4I(2I-1)\hbar} \tag{3}$$

for the asymmetry parameter $\eta = 0$, for example, in such a way as $\omega_1 = 6\omega_Q$, $\omega_2 = 12\omega_Q$, and $\omega_3 = 18\omega_Q$. In Eq. (3), the quadrupole moment of the probe nucleus on the relevant intermediate state of the cascade is $Q = +0.74(7)$ b [18], and the other symbols have usual meanings. It is to be noted that a normal distribution, δ, was included in fits of quadrupole frequencies for all perturbation functions in Fig. 5, with fitted values given in Table I.

The least-squares fit revealed that there coexist two different components (C1 and C2) in the room-temperature TDPAC function shown in Fig. 5(a), exhibiting distinct hyperfine interaction parameters as listed in Table I. The ω_Q and η values for C1 are greater than those for C2, signifying that the site of the dominant component C1 is largely distorted compared with C2 site. In the orthorhombic structure, the $Mn^{3+}O_6$ octahedra are regarded as distorted by the JT effect due to singly occupied e_g orbitals in Mn^{3+}, where polarons would be locally formed via the electron-lattice interaction [14,15]; whereas for $Mn^{4+}O_6$, the octahedra are not subject to the JT effect. Taking into consideration the fact that the fraction ratio of the components (f_{C1}/f_{C2}) shows agreement with the stoichiometric ratio of $Mn^{3+}/Mn^{4+} (= 0.7/0.3)$ in the present sample, we can assume that the degree of distortion of MnO_6 octahedra is directly related to the asymmetry (η) and the electric quadrupole frequency (ω_Q) at the ^{111}Cd probe nuclei forming C1 and C2. This interpretation is not applicable to a matrix in which Mn^{3+} and Mn^{4+} are randomly distributed in the lattice but to one in which Mn ions of different valences (Mn^{3+} and Mn^{4+}) individually form their aggregates, and the ^{111}Cd probes involved in each aggregate are perturbed by the different EFGs produced by the neighboring $Mn^{3+/4+}O_6$ octahedra. Stripe formation with alternate layers of Mn^{3+} and Mn^{4+} ions observed for $La_{0.7}Ca_{0.3}MnO_3$ [15,19] is consistent with this explanation; that is, this is an atomic-level observation of the polaron clusters from the viewpoint of the nonmagnetic La/Ca A site. [For the site assignment of the ^{111}Cd($\leftarrow {}^{111m}$Cd) probe, see the next section.]

As regards the low-temperature TDPAC functions shown in Figs. 5(b) and 5(c), the pattern is obviously different from that in Fig. 5(a) reflecting the phase transition below T_C. For the magnetic interaction between the magnetic moment of the probe nucleus and the hyperfine field, B_{hf}, the perturbation factor $G_{22}(t)$ is expressed with

$$G_{22}(t) = \tfrac{1}{5}[1 + 2\cos(\omega_L t) + 2\cos(2\omega_L t)], \tag{4}$$

where ω_L stands for the Larmor frequency, which is a function of B_{hf} in the following relation:

$$\omega_L \hbar = -g_N \mu_N B_{hf}. \tag{5}$$

Because of the low temperature measurement below T_C, the perturbation functions were fitted assuming the presence of both magnetic hyperfine field and EFG at the probe nucleus [10]. As a result, the upper limit value of the hyperfine field ($B_{hf} < 0.048$ T) was obtained as shown in Table I. Because of the negligibly small value, however, only the perturbation by the EFG is taken into account for the present multicomponent analyses for simplicity. (The small value is discussed in the next section.) From the fits, we found that only the C2 component survived but the oscillatory structure of C1 completely disappeared from both of the low-temperature functions. However, the amplitude of C2 does not change from that appearing in Fig. 5(a): namely, the disappeared C1 component does not contribute to the fractional increase of C2. For the analysis of the functions in Figs. 5(b) and 5(c), we fitted the data introducing an exponential function to the

TABLE I. Hyperfine interaction parameter values obtained by least-squares fits on the TDPAC functions of ^{111}Cd($\leftarrow {}^{111m}$Cd) in $La_{0.7}Ca_{0.3}MnO_3$.

Temp.	Comp.	ω_Q (Mrad s^{-1})	η	δ (%)	λ (10^8 s^{-1})	f(%)	B_{hf}(T)
R.T.	C1	21.0(1)	0.51(1)	14(1)	–	69(1)	–
	C2	14.0(1)	0.19(1)	12(1)	–	31(1)	–
201 K	C1	–	–	–	8.0(53)	63(5)	–
	C2	14.1(2)	0.09(1)	9(2)	–	39(5)	< 0.048
77 K	C1	–	–	–	4.1(9)	59(16)	–
	C2	14.0(1)	0.21(1)	12(1)	–	41(11)	< 0.048
4.2 K	Single	18.7(6)	0.41[a]	42(4)	–	100	–

[a]Fixed to the weighted mean value of η at room temperature.

perturbation factor assuming a fast relaxation of the probe nucleus for the C1 component [20]:

$$G_{22}(t) = f\exp(-\lambda t) + (1-f)\left[\sigma_{2,0} + \sum_{n=1}^{3}\sigma_{2,n}\cos(\omega_n t)\right]. \quad (6)$$

Here, λ denotes the relaxation constant for the C1 component. The results of the fit are also shown in Table I. The fast damping of C1 suggests that the static JT effect on the local lattice structure at temperature above T_C changed to a dynamic effect below T_C by the phase transition to the ferromagnetic metal. We understand this phenomenon to mean that delocalization of e_g electrons causes fluctuation of the local field of nearby lattice, which leads to dynamic perturbation to the adjacent ^{111}Cd probes. The time scale of the fluctuation can be deduced by the following relation between λ and the correlation time for the changes of the extranuclear field τ_c [10]:

$$\lambda = \frac{504}{5}\tau_c\omega_Q^2. \quad (7)$$

Using the ω_Q value at room temperature [$= 21.0(1)$ Mrad s^{-1}], the correlation time was evaluated to be $\tau_c = 1.8(12)\times 10^{-8}$ s at 77 K. We found from the result that the time scale of the fluctuation of the JT-distorted local lattice is slow enough to cause the fast nuclear spin relaxation of the probe.

The oscillatory structure in the perturbation function in Fig. 5(d) is distinct from those in Figs. 5(b) and 5(c). We analyzed the function assuming a single component with a wide distribution in the quadrupole frequency as listed in Table I. This result shows that the effect of the lattice distortion was spread to the whole system at this low temperature. The disappearance of the dynamic effect observed in the higher-temperature functions in Figs. 5(b) and 5(c) may signify freezing of the fluctuation of the polaronic local structures, suggesting that they can no longer follow the electron movement at this low temperature. The large distribution in the quadrupole frequencies may also be ascribable to the freezing of the fluctuation, resulting in random local structure. The obtained value of the quadrupole frequency, $\omega_Q = 18.7(6)$ Mrad s^{-1}, agrees well with the weighted mean value of those for C1 and C2 observed at room temperature, demonstrating the validity of the analysis.

2. *Magnetic hyperfine fields at the probes in the La/Ca A site*

For the site assignment of the ^{111}Cd($\leftarrow {}^{111m}$Cd) probes, it is natural to consider that they substitute for the A-site ions [21,22] because the ionic radius of Cd^{2+} (131 pm) in the dodecahedral coordination geometry is close to those of La^{3+} (136 pm) and Ca^{2+} (134 pm). This interpretation is corroborated by the magnitude of the magnetic hyperfine field (B_{hf}) at the probe site. The B_{hf} at the ^{111}Cd($\leftarrow {}^{111m}$Cd) probe site is vanishingly small (< 0.048 T) even at the temperature far below T_C. This small value provides an important clue to the probe site. If the ^{111}Cd($\leftarrow {}^{111m}$Cd) probe occupies the B site, a spin density would be fully transferred to the probe from Mn ions through oxygen p orbitals due to the bond angle of ^{111}Cd(B)–O–Mn close to 180°, and a considerably large supertransferred magnetic hyperfine field (SMHF) should be observed at the ^{111}Cd site [23–25]. Thus, the present small field provides circumstantial evidence that the ^{111}Cd($\leftarrow {}^{111m}$Cd) probe occupies the La/Ca A site which is connected to Mn through O at the bond angle of ^{111}Cd(A)–O–Mn close to 90°.

Then, what causes the marked change in the local field at the ^{140}Ce($\leftarrow {}^{140}$La) probe nucleus in the same A site below T_C($B_{hf} = 6.3(9)$ T at 240 K) [12]? There should be a distinct factor for the production of such a large field characteristic of the ^{140}Ce probe. We preliminarily proposed in our previous work [13] that the origin of the large field at the ^{140}Ce nucleus is the hyperfine interaction with a $4f$ spin slightly oriented by the small SMHF from adjacent Mn ions under ferromagnetic phase. The presence of a $4f$ electron signifies that the probe ion takes the trivalent state, $^{140}Ce^{3+}$, despite the fact that the parent of the probe, $^{140}La^{3+}$, emits a β^- particle in the nuclear decay process to transform into $^{140}Ce^{4+}$. Because the initial β^--decay product $^{140}Ce^{4+}$ is in the metal phase below T_C, the electron rearrangement in its atomic orbital presumably completes within 10^{-12} s through contribution of conduction electrons [10], resulting in reduction to the trivalent daughter $^{140}Ce^{3+}$ mostly before the first γ-ray emission of the cascade. [Note that the half-life of the initial state of the cascade on the 2412 keV level is as long as 55 ps [18]. See Fig. 1(b)]. The information provided during the time window of the observation is therefore of the perturbation to $^{140}Ce^{3+}$, where a $4f$ electron significantly contributes to the nuclear spin precession.

In relation to the effect of a $4f$ electron, incidentally, we should note the report that vanishing hyperfine fields of an upper limit of $0.3 \sim 0.4$ T were observed, even below the Néel temperatures, at the ^{140}Ce($\leftarrow {}^{140}$La) probe generated by the same nuclear reaction in antiferromagnetic perovskite compounds $LaCrO_3$ and $LaFeO_3$ [26]. This observation can be interpreted as meaning that the probe remains in the tetravalent $^{140}Ce^{4+}$ state in the conduction-electron free insulating phases over the time of observation, resulting in very small local magnetic fields produced at the ^{140}Ce probe, as observed for the present ^{111}Cd($\leftarrow {}^{111m}$Cd) probe.

IV. SUMMARY AND CONCLUSION

In the present work, the magnetic hyperfine field and/or EFGs at the ^{111}Cd($\leftarrow {}^{111m}$Cd) probe in a perovskite $La_{0.7}Ca_{0.3}MnO_3$ were measured by means of TDPAC spectroscopy to clarify the phenomenon locally occurring at the A site. Temperature dependence was observed for the TDPAC functions obtained above and below T_C. Two different components (C1 and C2) were detected in the room-temperature function: the C1 site is highly distorted and the C2 site less distorted; whereas at 201 and 77 K ($< T_C$), the oscillatory structure of C1 completely disappeared from the function. Taking the CMR property of the sample into consideration, we assigned C1 to the probes involved in aggregates of $Mn^{3+}O_6$ octahedra, which are highly distorted by the formation of polarons arising from the Jahn-Teller effect, and C2 to those of $Mn^{4+}O_6$ octahedra. The disappearance of the oscillatory structure of C1 below T_C is explained by the fast relaxation of the probe nucleus caused by fluctuation of the polaronic local lattice dragged by conduction electrons. At helium temperature, the TDPAC function consists of a single component with an averaged quadrupole frequency, indicating freezing of the fluctuation. It is interesting that the temperature variation of the local fields observed by the present ^{111}Cd probe is consistent with a recently reported phase diagram of $La_{1-x}Ca_xMnO_3$ [27].

The nonmagnetic ^{111}Cd($\leftarrow {}^{111m}$Cd) probe in the A site is magnetically perturbed at 77 K, but the field (SMHF from adjacent Mn ions) is vanishingly small ($B_{hf} < 0.048$ T), while the local field observed at the ^{140}Ce probe in the A site is significantly large at temperature below T_C. We conclude that the origin of the large field at the probe is the contribution of a $4f$ electron as in the trivalent state of $^{140}Ce^{3+}$. The large field has been preliminarily attributed to the orientation of a $4f$ spin by the SMHF from ferromagnetically ordered Mn ions due to the relatively large magnetic moment of the ^{140}Ce nucleus on the intermediate level; however, a possible effect of the nuclear quadrupole interaction with the EFG produced by a $4f$ electron on the large field also needs to be estimated for precise estimation of the hyperfine field.

ACKNOWLEDGMENTS

This work was supported in part by JSPS KAKENHI Grants No. 20612005, No. 26286075, and No. 18H03692, and was accomplished as part of Visiting Researcher's Program of Institute for Integrated Radiation and Nuclear Science, Kyoto University (KURNS). The authors are grateful to Prof. T. Takahashi of KURNS for his kind experimental support.

[1] S. Jin, T. H. Tiefel, M. McCormack, R. A. Fastnacht, R. Ramesh, and L. H. Chen, Science **264**, 413 (1994).
[2] A. P. Ramirez, J. Phys.: Condens. Matter **9**, 8171 (1997).
[3] C. Zener, Phys. Rev. **82**, 403 (1951).
[4] H. Y. Hwang, S-W. Cheong, P. G. Radaelli, M. Marezio, and B. Batlogg, Phys. Rev. Lett. **75**, 914 (1995).
[5] A. Moreo, S. Yunoki, and E. Dagotto, Science **283**, 2034 (1999).
[6] H. Zhang, K. Wang, Y. Zhang, W. Dong, L. Chen, X. Tang, and J. Chen, Appl. Phys. Lett. **111**, 192408 (2017).
[7] T. Terai, T. Sasaki, T. Kakeshita, T. Fukuda, T. Saburi, H. Kitagawa, K. Kindo, and M. Honda, Phys. Rev. B **61**, 3488 (2000).
[8] A. Urushibara, Y. Morimoto, T. Arima, A. Asamitsu, G. Kido, and Y. Tokura, Phys. Rev. B **51**, 14103 (1995).
[9] P. Schiffer, A. P. Ramirez, W. Bao, and S.-W. Cheong, Phys. Rev. Lett. **75**, 3336 (1995).
[10] H. Frauenfelder and R. M. Steffen, in *α-, β-, and γ-Ray Spectroscopy*, edited by K. Siegbahn (North-Holland, Amsterdam, 1965), Vol. 2, p. 997.
[11] G. Schatz and A. Weidinger, *Nuclear Condensed Matter Physics* (Wiley, New York, 1996).
[12] W. Sato, N. Ochi, A. Taniguchi, T. Terai, T. Kakeshita, A. Shinohara, and Y. Ohkubo, J. Nucl. Radiochem. Sci. **8**, 89 (2007).
[13] W. Sato, S. Komatsuda, A. Osa, T. K. Sato, and Y. Ohkubo, Hyperfine Interact. **237**, 113 (2016).
[14] A. J. Millis, P. B. Littlewood, and B. I. Shraiman, Phys. Rev. Lett. **74**, 5144 (1995).
[15] C. P. Adams, J. W. Lynn, Y. M. Mukovskii, A. A. Arsenov, and D. A. Shulyatev, Phys. Rev. Lett. **85**, 3954 (2000).
[16] V. Chechersky, A. Nath, I. Isaac, J. P. Franck, K. Ghosh, H. Ju, and R. L. Greene, Phys. Rev. B. **59**, 497 (1999).
[17] T. Terai, T. Kakeshita, T. Fukuda, T. Saburi, N. Takamoto, K. Kindo, and M. Honda, Phys. Rev. B. **58**, 14908 (1998).
[18] R. B. Firestone, in *Table of Isotopes*, 8th ed., edited by V. S. Shirley (Wiley, New York, 1996), Vol. 1.
[19] D. I. Khomskii and K. I. Kugel, Phys. Rev. B. **67**, 134401 (2003).
[20] For the disappearance of the oscillatory structure of C1, there is an alternate interpretation to the TDPAC functions that the ^{111}Cd probe nuclei are surrounded by widely distributed fields including extremely large EFG. However, it is difficult to explain the random distribution with an appropriate physical picture for the probe nuclei.
[21] A. M. L. Lopes, J. P. Araújo, J. J. Ramasco, V. S. Amaral, R. Suryanarayanan, and J. G. Correia, Phys. Rev. B **73**, 100408(R) (2006).
[22] A. M. L. Lopes, J. P. Araújo, V. S. Amaral, J. G. Correia, Y. Tomioka, and Y. Tokura, Phys. Rev. Lett. **100**, 155702 (2008).
[23] T. M. Rearick, G. L. Catchen, and J. M. Adams, Phys. Rev. B **48**, 224 (1993).
[24] G. L. Catchen, W. E. Evenson, and D. Allred, Phys. Rev. B **54**, R3679 (1996).

[25] R. L. Rasera and G. L. Catchen, Phys. Rev. B **58**, 3218 (1998).
[26] R. Dogra, A. C. Junquiera, R. N. Saxena, A. W. Carbonari, J. Mestnik-Filho, and M. Moralles, Phys. Rev. B **63**, 224104 (2001).
[27] N. Panopoulos, M. Pissas, H. J. Kim, J-G Kim, S. J. Yoo, J. Hassan, Y. AlWahedi, S. Alhassan, M. Fardis, N. Boukos, and G. Papavassiliou, npj Quantum Mater. **3**, 20 (2018).